The 8th European Congress on Computational Methods in Applied Sciences and Engineering
ECCOMAS Congress 2022
5-–9 June 2022, Oslo, Norway

MULTI-PHYSICAL MODELLING AND ANALYSIS OF LUBRICATED TRANSMISSIONS USING A COUPLED FINITE ELEMENT APPROACH

SANDER NEECKX[1,2], BART BLOCKMANS[1,2], WARD ROTTIERS[1,2] AND WIM DESMET[1,2]

[1] KU Leuven, Department of Mechanical Engineering,
Celestijnenlaan 300, B-3001, Heverlee, Belgium
e-mail: **sander.neeckx@kuleuven.be**

[2] DMMS Core lab, Flanders Make, Belgium

Key words: Multiphysics Problems, Flexible Multibody, TEHL, Monolithic Solver, Gears

Abstract. Lubrication is vital to improve performance, efficiency and durability in transmissions; it serves to minimize wear, noise, vibration and friction. The proper functioning of lubricated transmissions relies on interactions amongst a wide range of physical phenomena (contact dynamics, fluid-structure interaction and heat transfer) operating at different spatial and temporal scales. A lubricated transmission model is proposed in this work to obtain accurate information regarding all physical domains and the coupling thereof to quantify performance, efficiency and durability. The model consists of a thermo-elastically coupled flexible multibody model for the gear pair and a Thermo-Elasto-Hydrodynamic Lubrication (TEHL) model for the lubricant, both based on first principle modelling to ensure high fidelity.

1 INTRODUCTION

Lubricated transmissions are inherently multi-scale and multi-physical systems that are present in gearboxes of automotive applications, wind turbines and machines. Their proper functioning relies on the interactions amongst a wide range of physical phenomena (contact dynamics, fluid-structure interaction and heat transfer) operating at different spatial and temporal scales. Optimal lubrication is vital to improve performance, efficiency and durability in transmissions, since it improves the dynamic behaviour of the main components, such as gears and bearings. After all, it serves to minimize wear, noise, vibration and friction as a result of increased damping and reduced temperature at the contact zone. Nevertheless, an increasing temperature is inevitable in lubricated transmissions, resulting in thermal deformations that will influence the contact conditions, the pressure in the lubricant film and its temperature. Accurate prediction of dynamic stresses due to elastic deformations are crucial to reduce cost of ownership already at the design stage. For this purpose, accurate information regarding all physical domains and the coupling thereof is required to quantify performance, efficiency and durability.
The numerical model of lubricated transmission is twofold in spatial scale. First, global tooth deformations are computed at macroscopic scale with a thermo-elastically coupled flexible multibody model, thereby capturing root bending stresses. This model solves the second law of New-

ton [1] and Fourrier's law [2] to obtain elastic deformations with large rigid body motion and temperature, respectively. The second spatial scale is microscopic where local contact deformations are computed with a Thermo-Elasto-Hydrodynamic Lubriation (TEHL) model, thereby capturing local contact stress. This model solves Reynolds' equation [3, 4, 5] and the energy equation [5] to compute lubricant pressure and temperature, respectively, as well as Newton's second law for local elastic deformation.
The Finite Element Method (FEM) [6] is widely used to discretize all sorts of partial differential equations, which are multi-physically coupled in the aforementioned lubricated transmission model. Solving these discretized models remains a challenge due to the excessive amount of Degrees Of Freedom (DOFs), even for steady-state simulations. All DOFs are coupled due to the inherent mutual influence of one physical domain on the other. To cope correctly with these influences, iterative schemes are employed to solve the coupled nonlinear equilibrium equations, which adds further to the large overall computational complexity of the simulation. The highly complex multi-physically coupled lubricated transmission models, considered in this work, are not yet discretised with the FEM in literature, upon the authors best knowledge. The multi-physically coupled transmission model without thermal effects is already described in [7], albeit with semi-analytical methods instead of first-principle methods.
A.A. Shabana Outlines the theory of flexible multibody modelling in general [1], which is adopted by [8], resulting in a numerical model of a meshing gear pair. This work aims to extend the model with thermal deformations as outlined in [2] leading to a thermo-elastically coupled flexible multibody model. The outcome is a macroscopic scale model which is highly influencing the microscopic scale, due to changing contact conditions.
B. Tower observed experimentally that properly lubricated bodies in contact are completely separated by a thin lubricant film [9], which was firstly described with the famous Reynolds equation [3], setting the fundamentals of lubrication theory. It can be used as micro-scale model in flexible multi-body models, which are macroscopic scale, to compute contact forces [10]. Instead of coupling the EHL-model with a flexible multibody model, this work aims to combine the TEHL-model with a thermo-elastically coupled flexible multibody model. The TEHL-model, which is needed for accurate pressure prediction for highly loaded contacts, is well described in [5] for point contacts. The theory is similar for line contact in gears.
In this paper, two models are described to simulate the gear pair and lubricant, including thermal effects. The first model, computing the deformation and temperature distribution in the gear pair, is described in section 2; the second model, computing the pressure and heat flux in the lubricant, is described in section 3. Both models are subsequently coupled into the targeted lubricated transmission model in section 4. Numerical results are finally discussed in section 5.

2 THERMO-ELASTICALLY COUPLED FLEXIBLE MULTIBODY MODEL

A flexible multibody model, as the name suggests, defines a model of multiple deformable bodies, in casu two flexible gears in the application of gear contact. The Floating Frame of Reference (FFR) formulation [1] is adopted in this work to describe the elastodynamic behaviour of a flexible body subjected to large rigid body motion, though different formulations exist. A local reference frame is attached to each body in the system, as illustrated by Figure 1, which allows to distinguish between rigid body motion (translation and rotation of the local reference frame)

and small deformations. The latter is discretized with the FEM [6] in this model, resulting in constant mass and stiffness matrices. In addition, thermal deformations are incorporated in the flexible multibody model as an extra thermal force acting on the structure resulting into the thermo-elastically coupled flexible multibody model.

Generalized coordinates describe the rigid body motion and small deformations for each gear in the flexible multibody model. Given that only perfectly aligned gears are considered in this work, the considered generalized coordinates for gear i are limited to rigid body rotation along the Z-axis, $\theta^{(i)}$, and small deformations, $\bar{\boldsymbol{u}}^{(i)}$, expressed in the local reference frame $x^{(i)}y^{(i)}z^{(i)}$:

$$\boldsymbol{q}^{(i)} = \begin{bmatrix} \theta^{(i)} & \bar{\boldsymbol{u}}^{(i)^T} \end{bmatrix}^T \tag{1}$$

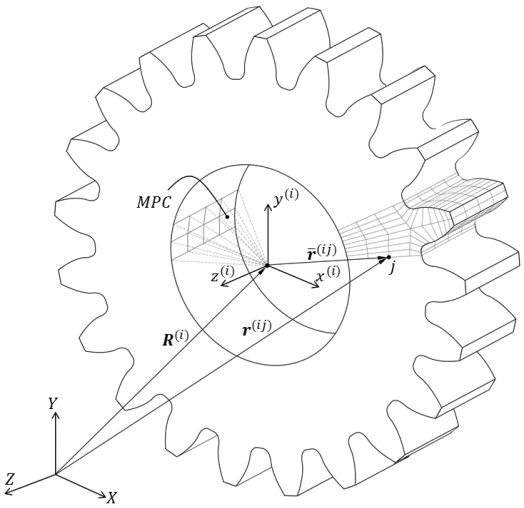

Figure 1: FFR fromulation for a flexible gear

2.1 Kinematic description of a material point

The position in the global reference frame, of node j on gear i can be expressed as:

$$\boldsymbol{r}^{(ij)} = \boldsymbol{R}^{(i)} + \boldsymbol{A}^{(i)}\bar{\boldsymbol{r}}^{(ij)} = \boldsymbol{R}^{(i)} + \boldsymbol{A}^{(i)}\left(\bar{\boldsymbol{r}}_0^{(ij)} + \bar{\boldsymbol{u}}^{(ij)}\right) = \boldsymbol{R}^{(i)} + \boldsymbol{A}^{(i)}\left(\bar{\boldsymbol{r}}_0^{(ij)} + \boldsymbol{I}^{(ij)}\bar{\boldsymbol{u}}^{(i)}\right) \tag{2}$$

where $\bar{\boldsymbol{r}}_0^{(ij)}$ represents the undeformed coordinates of node j on gear i expressed in the local reference frame, while the deformation is described by $\bar{\boldsymbol{u}}^{(i)}$ and $\boldsymbol{I}^{(ij)}$ resembles the row of the mapping matrix corresponding to node j on gear i. The transformation matrix $\boldsymbol{A}^{(i)}$ and its derivative depend on the Bryant angle $\theta^{(i)}$ and are defined for in plane motion as:

$$\boldsymbol{A}^{(i)} = \begin{bmatrix} \cos\left(\theta^{(i)}\right) & -\sin\left(\theta^{(i)}\right) & 0 \\ \sin\left(\theta^{(i)}\right) & \cos\left(\theta^{(i)}\right) & 0 \\ 0 & 0 & 1 \end{bmatrix}, \qquad \dot{\boldsymbol{A}}^{(i)} = \begin{bmatrix} -\sin\left(\theta^{(i)}\right) & -\cos\left(\theta^{(i)}\right) & 0 \\ \cos\left(\theta^{(i)}\right) & -\sin\left(\theta^{(i)}\right) & 0 \\ 0 & 0 & 0 \end{bmatrix} \dot{\theta}^{(i)} = \boldsymbol{B}^{(i)}\dot{\theta}^{(i)} \tag{3}$$

Differentiating equation (2) to time results in the velocity of node j on gear i expressed in the global reference frame:

$$\dot{\boldsymbol{r}}^{(ij)} = \boldsymbol{B}^{(i)}\bar{\boldsymbol{r}}^{(ij)}\dot{\theta}^{(i)} + \boldsymbol{A}^{(i)}\boldsymbol{I}^{(ij)}\dot{\tilde{\boldsymbol{u}}}^{(i)} = \begin{bmatrix}\boldsymbol{B}^{(i)}\bar{\boldsymbol{r}}^{(ij)} & \boldsymbol{A}^{(i)}\boldsymbol{I}^{(ij)}\end{bmatrix}\begin{bmatrix}\dot{\theta}^{(i)} \\ \dot{\tilde{\boldsymbol{u}}}^{(i)}\end{bmatrix} = \boldsymbol{L}^{(ij)}\left(\boldsymbol{q}^{(i)}\right)\dot{\boldsymbol{q}}^{(i)} \tag{4}$$

2.2 Kinetic energy and generalised forces of a flexible gear pair

Summing the kinetic energy of all n_n nodal point masses in the Finite Element (FE) model results in the total kinetic energy of gear i:

$$E_k^{(i)} = \sum_{j=1}^{n_n}\frac{1}{2}\dot{\boldsymbol{r}}^{(ij)^T}m^{(ij)}\dot{\boldsymbol{r}}^{(ij)} = \frac{1}{2}\dot{\boldsymbol{q}}^{(i)^T}\sum_{j=1}^{n_n}m^{(ij)}\begin{bmatrix}\bar{\boldsymbol{r}}^{(ij)^T}\bar{\boldsymbol{r}}_{xy}^{(ij)} & \bar{\boldsymbol{r}}^{(ij)^T}\boldsymbol{I}_{y-x}^{(ij)} \\ -\boldsymbol{I}^{(ij)^T}\bar{\boldsymbol{r}}_{y-x}^{(ij)} & \boldsymbol{I}^{(ij)^T}\boldsymbol{I}^{(ij)}\end{bmatrix}\dot{\boldsymbol{q}}^{(i)} \tag{5}$$

$$= \frac{1}{2}\dot{\boldsymbol{q}}^{(i)^T}\boldsymbol{M}^{(i)}\left(\boldsymbol{q}^{(i)}\right)\dot{\boldsymbol{q}}^{(i)} \tag{6}$$

where $\boldsymbol{M}^{(i)}$ is the multibody mass matrix, which depends on the state vector $\boldsymbol{q}^{(i)}$, $\blacksquare_{xy}$ symbolizes premultiplying with $\boldsymbol{B}^{(i)^T}\boldsymbol{B}^{(i)}$, while $\blacksquare_{y-x}$ symbolizes premultiplying with $\boldsymbol{B}^{(i)^T}\boldsymbol{A}^{(i)}$.

Summing the virtual work of the elastic forces from all n_e elements in the FE-model results in the total virtual work of the elastic forces:

$$\delta W_f^{(i)} = \sum_{e=1}^{n_e} -\int_{V^{(ie)}}\left(\sigma_M^{(ie)^T} + \sigma_T^{(ie)^T}\right)\delta\epsilon^{(ie)}dV^{(ie)} \tag{7}$$

where σ_M is the stress resulting from mechanical forces, while σ_T results from thermal forces and ϵ denotes the strain. Furhter evaluation results in:

$$\delta W_f^{(i)} = -\boldsymbol{q}^{(i)^T}\begin{bmatrix}0 & 0 \\ 0 & \boldsymbol{K}_{FE}^{(i)^T}\end{bmatrix}\delta\boldsymbol{q}^{(i)} - \boldsymbol{T}^{(i)^T}\begin{bmatrix}0 & \boldsymbol{K}_{TM,FE}^{(i)^T}\end{bmatrix}\delta\boldsymbol{q}^{(i)} \tag{8}$$

$$= -\boldsymbol{q}^{(i)^T}\boldsymbol{K}^{(i)^T}\delta\boldsymbol{q}^{(i)} - \boldsymbol{T}^{(i)^T}\boldsymbol{K}_{TM}^{(i)^T}\delta\boldsymbol{q}^{(i)} = \boldsymbol{Q}_f^{(i)^T}\left(\boldsymbol{q}^{(i)}, \boldsymbol{T}^{(i)}\right)\delta\boldsymbol{q}^{(i)} \tag{9}$$

where $\boldsymbol{K}_{FE}^{(i)}$ and $\boldsymbol{K}_{TM,FE}^{(i)}$ are the FE-matrices introducting stiffness and thermo-elastic coupling [6, 2], respectively. $\boldsymbol{Q}_f^{(i)}$ is the total virtual energy resulting from elastic forces on gear i, which depends on the state vectors $\boldsymbol{q}^{(i)}$ and $\boldsymbol{T}^{(i)}$. Including the generalized external forces $\boldsymbol{Q}_{ex}^{(i)}$ and generalized contact forces $\boldsymbol{Q}_c^{(i)}$ results into the total generalized forces $\boldsymbol{Q}^{(i)}$ on gear i.

2.3 Equations Of Motion (EOMs) of a flexible gear pair

Lagrange's equation of an unconstrained system allows to derive the EOMs from gear i:

$$\frac{d}{dt}\left(\frac{\partial E_k^{(i)}}{\partial\dot{\boldsymbol{q}}^{(i)}}\right)^T - \left(\frac{\partial E_k^{(i)}}{\partial\boldsymbol{q}^{(i)}}\right)^T = \boldsymbol{Q}^{(i)} \tag{10}$$

$$\boldsymbol{M}^{(i)}\left(\boldsymbol{q}^{(i)}\right)\ddot{\boldsymbol{q}}^{(i)} + \boldsymbol{K}^{(i)}\boldsymbol{q}^{(i)} + \boldsymbol{K}_{TM}^{(i)}\boldsymbol{T}^{(i)} = \boldsymbol{Q}_{ex}^{(i)} + \boldsymbol{Q}_c^{(i)}\left(\boldsymbol{q}^{(i)}, \boldsymbol{T}^{(i)}\right) + \boldsymbol{Q}_v^{(i)}\left(\boldsymbol{q}^{(i)}, \dot{\boldsymbol{q}}^{(i)}\right) \tag{11}$$

where the quadratic velocity term $\boldsymbol{Q}_v^{(i)}$ is defined as:

$$\boldsymbol{Q}_v^{(i)}\left(\boldsymbol{q}^{(i)},\dot{\boldsymbol{q}}^{(i)}\right) = -\sum_{j=1}^{n_n} m^{(ij)} \begin{bmatrix} \dot{\bar{\boldsymbol{u}}}^{(i)^T}\boldsymbol{I}^{(ij)^T}\left(2\dot{\theta}^{(i)}\bar{\boldsymbol{r}}_{xy}^{(ij)} + \boldsymbol{I}_{y-x}^{(ij)}\dot{\bar{\boldsymbol{u}}}^{(i)}\right) \\ -\dot{\theta}^{(i)}\boldsymbol{I}^{(ij)^T}\left(\dot{\theta}^{(i)}\bar{\boldsymbol{r}}_{xy}^{(ij)} + 2\boldsymbol{I}_{y-x}^{(ij)}\dot{\bar{\boldsymbol{u}}}^{(i)}\right) \end{bmatrix} \tag{12}$$

and the temperature is computed from the heat transfer equation:

$$\boldsymbol{C}_T^{(i)}\dot{\boldsymbol{T}}^{(i)} + \boldsymbol{K}_T^{(i)}\boldsymbol{T}^{(i)} = \boldsymbol{Q}_{c,T}^{(i)}\left(\boldsymbol{q}^{(i)},\boldsymbol{T}^{(i)}\right) \tag{13}$$

where $\boldsymbol{C}_T^{(i)}$ and $\boldsymbol{K}_T^{(i)}$ are the FE-matrices introducing thermal capacity and conductivity [2], respectively. $\boldsymbol{Q}_{c,T}^{(i)}$ is the heat flux resulting from the contact interaction of two gear flanks. Solving this strongly coupled system requires an iterative solution strategy. However, the dynamic response of the thermal domain is significantly slower compared to the dynamic response of structural deformations allowing a weakly coupled system. Equations (11) and (13) are solved for each timestep in a dynamic simulation where the thermal load in equation (11) is lagging one timestep behind.

3 THERMO-ELASTO-HYDRODYNAMIC LUBRICATION (TEHL) MODEL

The isothermal Elasto-Hydrodynamic Lubrication (EHL)-model [4] couples Reynolds' equation, the elastic deformation equation and the load balance equation. The Reynolds equation is 1D for line contact in gears, as the pressure across the film thickness and along the contact line is constant. However, temperature is not constant across the film thickness in the TEHL-model [5], implying a 2D energy equation and a generalized Reynolds equation. The latter takes into account the temperature variation across the film thickness for usage in the TEHL-model together with the elastic deformation equation, the load balance equation and the energy equation.

3.1 Generalized Reynolds equation

The generalized Reynolds equation extends the classical Reynolds equation by permitting variation of the lubricant parameters along the film, but across the film thickness as well, requiring a mean pressure $\bar{p}$ across the film thickness. The derivation of the generalized Reynolds equation [11] for line contact is based on the compressible momentum equations (Navier-Stokes) in 2D, as is the case for the classical Reynolds equation [4]. Reducing the computational complexity of the Navier-Stokes equations is feasible with three assumptions since (i) the film thickness dimension is significantly smaller than the length of the lubricated surfaces, (ii) inertia-terms are negligible, and (iii) body forces are negligible. The approximated equation is only 1D in the direction of the lubricated surfaces, since the momentum equation across the film thickness is neglected:

$$\frac{\partial \bar{p}}{\partial x} = \frac{\partial}{\partial z}\left(\eta^{lub}\frac{\partial u}{\partial z}\right) \tag{14}$$

where η^{lub} is the lubricant viscosity and u is the lubricant velocity. Integrating equation (14) over the film thickness, and taking into account the boundary conditions, results into an expression

for the velocity component in function of the film thickness direction z:

$$u\left(z\right) = U_1 + \frac{\partial \bar{p}}{\partial x}\int_0^z \frac{z^{'}}{\eta^{lub}}dz^{'} + \left(\eta_e^{lub}\left(U_2 - U_1\right) - \frac{\eta_e^{lub}}{\eta_e^{lub'}}\frac{\partial \bar{p}}{\partial x}\right)\int_0^z \frac{1}{\eta^{lub}}dz^{'} \tag{15}$$

where U_1 and U_2 are the tangential boundary velocities of the upper and lower body, respectively. η_e^{lub} and $\eta_e^{lub'}$ are parameters that require integration across the film thickness and are defined as follows:

$$\frac{1}{\eta_e^{lub}} = \int_0^h \frac{1}{\eta^{lub}}dz, \qquad \frac{1}{\eta_e^{lub'}} = \int_0^h \frac{z}{\eta^{lub}}dz \tag{16}$$

where h is the film thickness of the lubricant and all integrals across the film thickness are evaluated using Simpson's integration rule, based on the values of previous iteration.
The last step to end up with the generalized Reynolds equations involves integrating the continuity equation across the film thickness and inserting equation (15). A stable TEHL-solver is assured by using dimensionless variables, which are based upon Hertzian contact parameters (contact half-width a and maximum contact pressure p_h) and parameters at ambient conditions (density ρ_R^{lub} and viscosity η_R^{lub}). The dimensionless variables are chosen as follows: $X = {}^{x}/_{a}$, $Z = {}^{z}/_{h}$, $\bar{\rho}^{lub} = {}^{\rho^{lub}}/_{\rho_R^{lub}}$, $\bar{\eta}^{lub} = {}^{\eta^{lub}}/_{\eta_R^{lub}}$, $P = {}^{\bar{p}}/_{p_h}$ and $H = {}^{hR_{eq}}/_{a^2}$, such that the resulting dimensionless generalized Reynolds equation is defined as:

$$\frac{\partial}{\partial X}\left(\bar{\epsilon}^{lub'}\frac{\partial P}{\partial X}\right) = \frac{\partial}{\partial X}\left(\bar{\rho}^{lub^*}H\right) \tag{17}$$

where:

$$\bar{\epsilon}^{lub'} = \frac{p_h a^3 H^3}{\eta_R^{lub} R_{eq}^2}\left(\frac{\bar{\rho}}{\bar{\eta}}\right)_e^{lub} = \frac{H^3}{\lambda^{'}}\left(\frac{\bar{\rho}}{\bar{\eta}}\right)_e^{lub}, \qquad \bar{\rho}^{lub^*} = U_1\bar{\rho}_e^{lub} + \left(U_2 - U_1\right)\bar{\eta}_e^{lub}\bar{\rho}_e^{lub'} \tag{18}$$

$$\left(\frac{\bar{\rho}}{\bar{\eta}}\right)_e^{lub} = \frac{\bar{\eta}_e^{lub}}{\bar{\eta}_e^{lub'}}\bar{\rho}_e^{lub'} - \bar{\rho}_e^{lub''}, \qquad \frac{1}{\bar{\eta}_e^{lub}} = \int_0^1 \frac{1}{\bar{\eta}^{lub}}dZ, \qquad \frac{1}{\bar{\eta}_e^{lub'}} = \int_0^1 \frac{Z}{\bar{\eta}^{lub}}dZ \tag{19}$$

$$\bar{\rho}_e^{lub} = \int_0^1 \bar{\rho}^{lub}dZ, \qquad \bar{\rho}_e^{lub'} = \int_0^1 \bar{\rho}^{lub}\int_0^Z \frac{dZ^{'}}{\bar{\eta}^{lub}}dZ, \qquad \bar{\rho}_e^{lub''} = \int_0^1 \bar{\rho}^{lub}\int_0^Z \frac{Z^{'}dZ^{'}}{\bar{\eta}^{lub}}dZ \tag{20}$$

3.2 Film thickness equation

The dimensionless film thickness H, used in the generalized Reynolds equation, is computed from the penetration depth from both undeformed contacting surfaces H_0, the undeformed geometry of the contacting surfaces (approximated as a parabola, based on the radius of curvature) and its local deformation $\bar{\delta}$ due to the pressure distribution in the lubricant film:

$$H\left(X\right) = H_0 + \frac{X^2}{2} + \bar{\delta}\left(X\right) \tag{21}$$

3.3 Load balance equation

The pressure distribution in the lubricant film supports the externally applied load, which is used to compute the Hertzian contact parameters to retrieve the dimensionless equations.

Hence, the dimensionless load balance equation reduces to:

$$\int_{-\infty}^{\infty} P\left(X\right) dX = \frac{\pi}{2} \tag{22}$$

3.4 Energy equation

The energy equation computes thermal effects in the lubricant film, which are mainly caused by shear pressure, while compressive heating is neglected. Heat transport is dominated by conduction in the lubricant film thickness and convection along the lubricant film, while conduction and convection in the other directions is negligible. As for the generalized Reynolds equation, using dimensionless variables in the energy equation assures a stable TEHL-solver. The resulting dimensionless energy equation, using the dimensionless temperature $\bar{T} = {}^{T}/_{T_R}$, is defined as in [5]:

$$-\frac{\partial}{\partial Z}\left(\bar{k}_T^{lub}\frac{\partial \bar{T}}{\partial Z}\right) + \bar{\rho}\bar{c}_T^{lub}\bar{u}\frac{\partial T}{\partial X} = \bar{\eta}^{lub}\left(\frac{\partial \bar{u}}{\partial Z}\right)^2 \tag{23}$$

where:

$$\bar{k}_T^{lub} = \frac{k_T^{lub}T_0}{\eta_R^{lub}}, \qquad \bar{c}_T^{lub} = \frac{\rho_R^{lub}c_T^{lub}T_0 a^3 H^2}{\eta_R^{lub}R_{eq}^2} \tag{24}$$

$$\bar{u} = U_1 + \frac{H^2}{\lambda'}\frac{\partial P}{\partial X}\int_0^Z \frac{Z'}{\bar{\eta}^{lub}}dZ' + \left(\bar{\eta}_e^{lub}\left(U_2 - U_1\right) - \frac{H^2}{\lambda'}\frac{\bar{\eta}_e^{lub}}{\bar{\eta}_e^{lub\prime}}\frac{\partial P}{\partial X}\right)\int_0^Z \frac{1}{\bar{\eta}^{lub}}dZ' \tag{25}$$

$$\frac{\partial \bar{u}}{\partial Z} = \frac{H^2}{\lambda'}\frac{\partial P}{\partial X}\frac{Z}{\bar{\eta}^{lub}} + \left(\bar{\eta}_e^{lub}\left(U_2 - U_1\right) - \frac{H^2}{\lambda'}\frac{\bar{\eta}_e^{lub}}{\bar{\eta}_e^{lub\prime}}\frac{\partial P}{\partial X}\right)\frac{1}{\bar{\eta}^{lub}} \tag{26}$$

with k_T^{lub} as the thermal conductivity coefficient and c_T^{lub} as the thermal heat capacity.

3.5 Lubricant rheology

The rheological parameters η^{lub} and ρ^{lub} of the lubricant are not constant in TEHL-modelling since compressibility of the lubricant is not negligible at high pressure values ($\sim$ 0.01-3 GPa). In this work, empirical laws are used to model the variation in rheological parameters due to their simplicity and good correspondance with measurements for moderate pressure values ($<$ 1 GPa). Among the wide variaty of models available, the model proposed by Roelands [12] is adopted to evaluate viscosity variations:

$$\eta^{lub} = \eta_R^{lub}\exp\left(\left(\ln\left(\eta_R^{lub}\right) + 9.67\right)\left[\left(1 + 5.1\cdot 10^{-9}p\right)^Z\left(\frac{T-138}{T_R-138}\right)^{-S} - 1\right]\right) \tag{27}$$

where:

$$Z = \frac{\alpha_{VP}^{lub}}{5.1\cdot 10^{-9}\left(\ln\left(\eta_R^{lub}\right) + 9.67\right)}, \qquad S = \frac{\beta_{VT}^{lub}\left(T_R - 138\right)}{\ln\left(\eta_R^{lub}\right) + 9.67} \tag{28}$$

and α_{VP}^{lub} and β_{VT}^{lub} depend on the type of lubricant.
Density variations are evaluated with the model proposed by Dowson & Higginson [13]:

$$\rho^{lub} = \rho_R^{lub}\left[1 + \frac{0.6 \cdot 10^{-9} p}{1 + 1.7 \cdot 10^{-9} p} - \beta_{DT}^{lub}\left(T - T_R\right)\right] \tag{29}$$

where β_{DT}^{lub} depends on the type of lubricant.

4 LUBRICATED TRANSMISSION MODEL

Coupling of the thermo-elastically coupled flexible multibody model (section 2) with the TEHL-model (section 3), to compute macroscopic and microscopic deformations, results into the lubricated transmission model. The TEHL-model cannot be readily used in this coupled framework as it needs a known total contact force F_c, in order to make the system dimensionless, which is generally not known in gear contact. Algorithm 1 computes the unknown contact force, which introduces an iterative loop over the (iterative) TEHL-solver to match its penetration depth h_0 with that of the locally undeformed gear flanks δ_{pen}.

Algorithm 1 Contact force computation from TEHL-model with known penetration depth H_0

Input: Penetration depth from locally undeformed gear flanks in contact δ_{pen} and estimate of total contact force F_c

Output: Distributed $\boldsymbol{F}$ and total F_c contact force resulting from the pressure distribution in the TEHL-model

for i = 1 to $Max.\ iterations$ **do**
  Compute Hertzian parameters a & p_h based on F_c
  Compute the penetration depth H_0 from the (iterative) TEHL-solver ($h_0 = {}^{H_0 a^2}/_{R_{eq}}$)
  Compute residual: $Res = \delta_{pen} - h_0$
  if $Res < tol$ **then**
    Break
  else
    Compute Jacobian: $Jac = \frac{\partial Res}{\partial F_c} = -\frac{\partial h_0}{\partial F_c} \approx -\frac{h_0(F_c+\Delta F_c) - h_0(F_c)}{\Delta F_c}$
    Update total contact force: $F_c = F_c - Jac^{-1} \cdot Res$
  end if
end for

The deformation of gear teeth, contact forces due to lubricant pressure and externally applied torque must be matched for steady-state equilibrium in gear contact. Algorithm 2 illustrates the lubricated transmission model for steady-state equilibrium, which consist of three nested iterative loops ((i) iterative TEHL-solver, (ii) contact force from TEHL-model with known penetration depth & (iii) match gear deflection with lubricant force), where the Jacobian of the contact forces is computed via the finite difference method.

Algorithm 2 Steady-state lubricated transmission model

Input: Stiffness matrices $\boldsymbol{K}_{FE}^{(i)}$, torque $T^{(1)}$, deformation resulting from steady-state dry contact equilibrium $\bar{\boldsymbol{u}}^{(i)}$ and corresponding angular configuration $\theta^{(1)}$ of gear 1.
Output: Deformation resulting from steady-state lubricated contact equilibrium $\bar{\boldsymbol{u}}^{(i)}$ and corresponding angular configuration $\theta^{(1)}$ of gear 1.

1: **for** i = 1 to $Max.\ iterations$ **do**
2: Compute contact force from deformation: $\boldsymbol{F}^{(i)} = \boldsymbol{K}_{FE}^{(i)} \bar{\boldsymbol{u}}^{(i)}$
3: Compute global deformation of gear tooth (ommit local deformation) [14]
4: Compute contact force from TEHL-model with know penetration depth (Algorithm 1)
5: Project distributed contact force resulting from TEHL-model on gear flank
6: Construct generelized force vectors $Q_{c,\theta}^{(1)}(\boldsymbol{q})$, $\boldsymbol{Q}_{c,u}^{(1)}(\boldsymbol{q})$ & $\boldsymbol{Q}_{c,u}^{(2)}(\boldsymbol{q})$
7: Compute residual: $\boldsymbol{Res} = \begin{bmatrix} 0 & \mathbf{0} & \mathbf{0} \\ \mathbf{0} & \boldsymbol{K}_{FE}^{(1)} & \mathbf{0} \\ \mathbf{0} & \mathbf{0} & \boldsymbol{K}_{FE}^{(2)} \end{bmatrix} \begin{bmatrix} \theta^{(1)} \\ \bar{\boldsymbol{u}}^{(1)} \\ \bar{\boldsymbol{u}}^{(2)} \end{bmatrix} - \begin{bmatrix} T^{(1)} \\ \mathbf{0} \\ \mathbf{0} \end{bmatrix} - \begin{bmatrix} Q_{c,\theta}^{(1)}(\boldsymbol{q}) \\ \boldsymbol{Q}_{c,u}^{(1)}(\boldsymbol{q}) \\ \boldsymbol{Q}_{c,u}^{(2)}(\boldsymbol{q}) \end{bmatrix}$
8: **if** $||\boldsymbol{Res}|| < tol$ **then**
9: Break
10: **else**
11: Compute Jacobian: $\boldsymbol{Jac} = \frac{\partial \boldsymbol{Res}}{\partial \boldsymbol{q}} = \begin{bmatrix} 0 & \mathbf{0} & \mathbf{0} \\ \mathbf{0} & \boldsymbol{K}_{FE}^{(1)} & \mathbf{0} \\ \mathbf{0} & \mathbf{0} & \boldsymbol{K}_{FE}^{(2)} \end{bmatrix} - \begin{bmatrix} \frac{\partial Q_{c,\theta}^{(1)}}{\partial \theta^{(1)}} & \frac{\partial Q_{c,\theta}^{(1)}}{\partial \bar{\boldsymbol{u}}^{(1)}} & \frac{\partial Q_{c,\theta}^{(1)}}{\partial \bar{\boldsymbol{u}}^{(2)}} \\ \frac{\partial \boldsymbol{Q}_{c,u}^{(1)}}{\partial \theta^{(1)}} & \frac{\partial \boldsymbol{Q}_{c,u}^{(1)}}{\partial \bar{\boldsymbol{u}}^{(1)}} & \frac{\partial \boldsymbol{Q}_{c,u}^{(1)}}{\partial \bar{\boldsymbol{u}}^{(2)}} \\ \frac{\partial \boldsymbol{Q}_{c,u}^{(2)}}{\partial \theta^{(1)}} & \frac{\partial \boldsymbol{Q}_{c,u}^{(2)}}{\partial \bar{\boldsymbol{u}}^{(1)}} & \frac{\partial \boldsymbol{Q}_{c,u}^{(2)}}{\partial \bar{\boldsymbol{u}}^{(2)}} \end{bmatrix}$
12: Update state vector $\boldsymbol{q}$: $\begin{bmatrix} \theta^{(1)} \\ \bar{\boldsymbol{u}}^{(1)} \\ \bar{\boldsymbol{u}}^{(2)} \end{bmatrix} = \begin{bmatrix} \theta^{(1)} \\ \bar{\boldsymbol{u}}^{(1)} \\ \bar{\boldsymbol{u}}^{(2)} \end{bmatrix} - \boldsymbol{Jac}^{-1} \cdot \boldsymbol{Res}$
13: **end if**
14: **end for**

5 NUMERICAL RESULTS

All numerical experiments are conducted on the same lubricated gear pair at steady-state equilibrium. A globally rigid, but locally flexible gear pair is considered in section 5.1, while a fully flexible one is dealt with in section 5.2.

5.1 TEHL-model

The TEHL-model is applied to a globally rigid, but locally flexible gear pair from which the radius of curvature at the contact point and the corresponding contact force are computed analytically. An angular configuration with two teeth pair in contact is considered. The contact point of the first tooth pair is close to the pitch point (where pure rolling motion occurs), and further from the pitch point for the second tooth pair. The difference in sliding velocity between both gear flanks is higher for the latter case, leading to higher shear forces and more lubricant heat-up, as illustrated in Figure 2.

A simulation with the (dry) Hertzian contact model and the Elasto-Hydrodynamic Lubrication

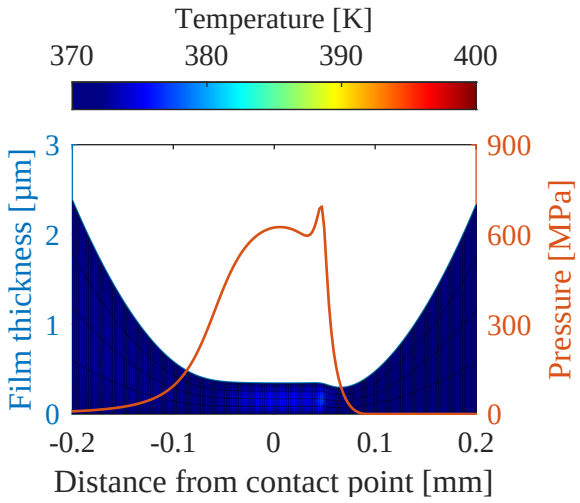

(a) Contact of first tooth pair close to pitch point, with a contact force of 1585N and a radius of curvature of 16.91mm (11.82mm) for gear 1 (2)

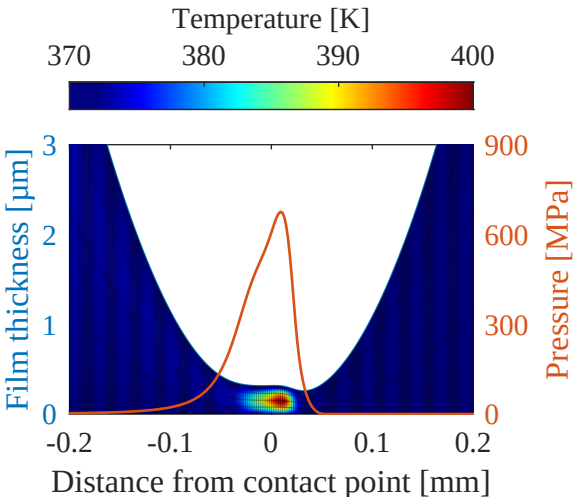

(b) Contact of second tooth pair furhter from pitch point, with a contact force of 781N and a radius of curvature of 5.10mm (23.63mm) for gear 1 (2)

Figure 2: TEHL-solution of a globally rigid, but locally flexible gear pair

(EHL) model is conducted as well in Figure 3 to showcase the need of the TEHL-model in gear contact. The difference in friction coefficient between dry and lubricated contact proves without any doubt the need of lubrication, while the need of the TEHL-model is only apparent for the contact further from the pitch point where lubricant heat-up causes an overestimation of the friction coefficient by the EHL-model.

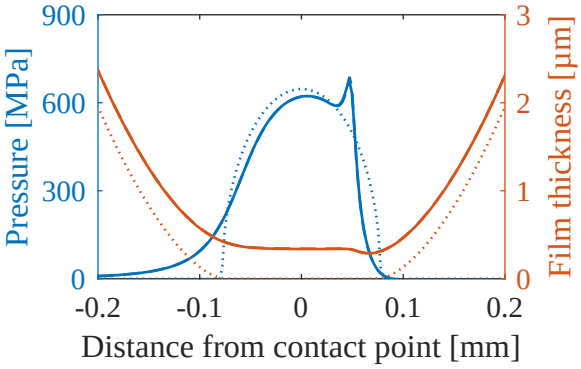

(a) Contact of first tooth pair close to pitch point, with average friction coefficient of 0.4, 0.021 and 0.019 for the Hertzian (dotted line), EHL- (dashed line) and TEHL-model (solid line), respectively

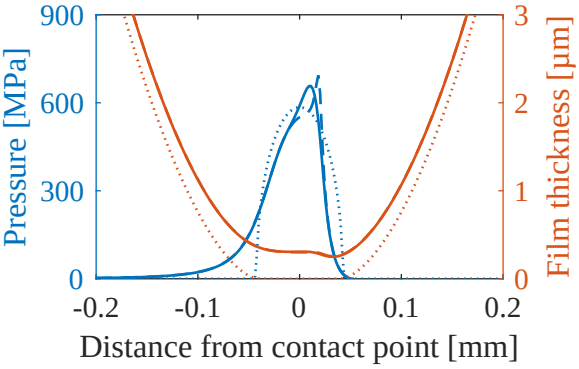

(b) Contact of second tooth pair further from pitch point, with average friction coefficient of 0.4, 0.066 and 0.035 for the Hertzian (dotted line), EHL- (dashed line) and TEHL-model (solid line), respectively

Figure 3: Comparison of the Hertzian, EHL- and TEHL-model applied on the rigd gear geometry

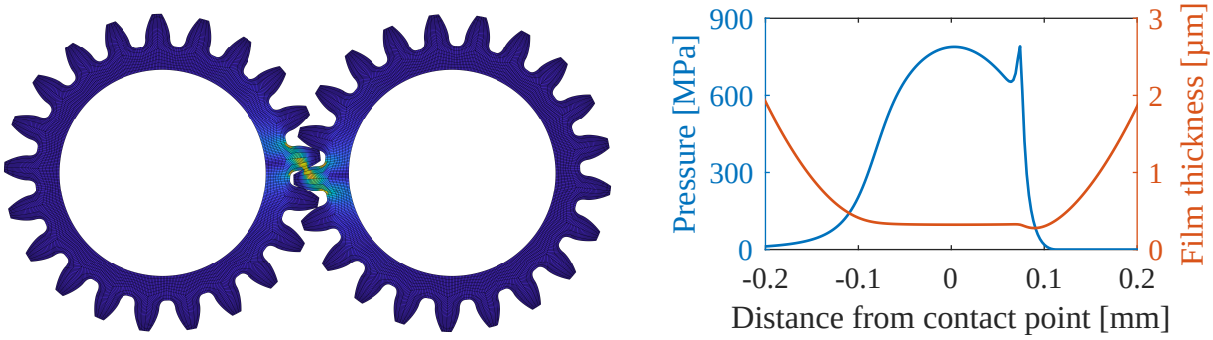

(a) Stresses in flexible gear geometry

(b) Pressure and film thickness

Figure 4: Numerical result of the lubricated transmission model

5.2 Lubricated transmission model

The EHL-model is coupled with a steady-state flexible gear pair for contact close to the pitch point, since it provides a good estimate of the friction coefficient if the difference in sliding velocity between both gear flanks is not too high. An angular configuartion with only one tooth pair in contact is considered to fulfill latter condition, while a coupling with the TEHL-model is required for an increasing difference in sliding velocity. The resulting stress in the gear pair and the corresponding pressure distribution and film thickness are shown in Figure 4.

Algorithms 1 and 2 were successfully adopted to obtain the converged steady-state equilibrium of a lubricated gear pair, where the driven gear is clamped such that the angular configuration of the driving gear matches the lubricant pressure (contact force) and elastic deformation with the applied torque. The model is quite expensive as the contact-Jacobian is computed by employing the finite difference methods, such that the EHL-model needs to be evaluated for every column in the contact-Jacobian. Nevertheless, only the relevant nodes at the contact zone are taken into account and the EHL-solution from the residual is reused as initial guess to speed up the assembly of the contact-Jacobian.

6 CONCLUSIONS AND FUTURE WORK

The high-fidelity lubricated transmission model introduced in this work reveals the challenges to couple a thermo-elastically coupled flexible multibody model for the gear pair and a TEHL-model for the lubricant. Three nested iterative loops are needed to develop a stable solver that converges to steady-state equilibrium. First principle modelling is adopted to ensure high fidelity, implying a considerable computational cost due to the nonlinearities in the model. Future work will focus on the development of a Reduced-Order-Model (ROM) to enable dynamic simulations, allowing the quantification of dynamic phenomena.

7 Aknowledgments

The Research Foundation - Flanders (FWO) is gratefully acknowledged for its support through research grant no. 1SD5721N.

REFERENCES

[1] A. A. Shabana, *Dynamics of Multibody Systems*, 4th ed. New York, USA: Cambridge University Press, 2013.

[2] R. B. Hetnarski and M. R. Eslami, *Thermal Stresses - Advanced Theory and Applications*. Springer, 2009, vol. 158.

[3] O. Reynolds, "On the Theory of Lubrication and its Application to Mr. Beauchamp Tower's Experiments, including an Experimental Determination of the Viscosity of Olive Oil," *Philosophical Transactions of the Royal Society of London*, vol. 177, pp. 157–234, 1885.

[4] B. J. Hamrock, S. R. Schmid, and B. O. Jacobson, *Fundamental of Fluid Film Lubrication*, 2nd ed. New York, USA: Marcel Dekker, Inc., 2004.

[5] W. Habchi, D. Eyheramendy, S. Bair, P. Vergne, and G. Morales-Espejel, "Thermal elastohydrodynamic lubrication of point contacts using a Newtonian/generalized Newtonian lubricant," *Tribology Letters*, vol. 30, no. 1, pp. 41–52, 2008.

[6] T. J. Hughes, *The finite element method - Linear static and dynamic finite element analysis*. New Jersey, USA: Prentice-Hall, Inc., 1987.

[7] L. Scurria, T. Tamarozzi, P. Jiránek, and D. Fauconnier, "A transient EHL contact model capturing system-level spur gears dynamic behavior," in *Proceedings of the 5 th Joint International Conference on Multibody System Dynamics*, Lisboa, Portugal, 2018.

[8] B. Blockmans, T. Tamarozzi, F. Naets, and W. Desmet, "A nonlinear parametric model reduciton method for efficient gear contact simulations," *International Journal for Numerical Methods in Engineering*, vol. 102, pp. 1162–1191, 2015.

[9] B. Tower, "First report on friction experiments," *Proceedings of the institution of mechanical engineers*, vol. 34, no. 1, pp. 632–659, 1883.

[10] A. Krinner, T. Schindler, and D. J. Rixen, "Time integration of mechanical systems with elastohydrodynamic lubricated joints using Quasi-Newton method and projection formulations," *International Journal for Numerical Methods in Engineering*, vol. 110, no. 6, pp. 523–548, 2017.

[11] D. Dowson, "A generalized Reynolds equation for fluid-film lubrication," *International Journal of Mechanical Sciences*, vol. 4, no. 2, pp. 159–170, 1962.

[12] C. J. A. Roelands, "Correlational Aspects of the Viscosity-Temperature Pressure Relationship of Lubricating Oils," Ph.D. dissertation, TU Delft, 1966.

[13] D. Dowson and G. R. Higginson, *Elasto-hydrodynamic lubrication: the fundamentals of roller and gear lubrication*. Oxford, UK: Pergamon Press, 1966.

[14] N. Cappellini, T. Tamarozzi, B. Blockmans, J. Fiszer, F. Cosco, and W. Desmet, "Semi-analytic contact technique in a non-linear parametric model order reduction method for gear simulations," *Meccanica*, vol. 53, no. 1-2, pp. 49–75, 2018.